Rate constants for quenching the $\tilde{A}\,^2A_2$ state of SO_2^+ by atmospheric gases

Timothy F. Thomas
Department of Chemistry, University of Missouri-Kansas City, Kansas City, Missouri 64110
Fred Dale and John F. Paulson
Air Force Geophysics Laboratory/LID, Hanscom AFB, Massachusetts 01731

(Received 11 August 1987; accepted 13 January 1988)

The effect of ion source pressure on the cross sections for photodissociation of SO_2^+ has been measured systematically at $\lambda_{irr} = 4735$ and 4795 Å. Using a Stern-Volmer treatment modified to account for the dependence of source residence time on pressure, rate constants have been measured for quenching the $\tilde{A}\,^2A_2$ $(v_1,v_2 = 3,3)$ and $\tilde{A}\,^2A_2(v_1,v_2 = 3,0)$ states of SO_2^+ by N_2O, SO_2, CO_2, and N_2. With SO_2 and N_2O as quenchers the rate constants range between 1.0 and 6.5 times the theoretical thermal capture rate constants ("Langevin limit"). The occurrence of several resonant and many near-resonant charge transfer processes is proposed to explain the unusually large rate constants.

I. INTRODUCTION

In the course of obtaining the ion photodissociation spectrum of SO_2^+, which we have recently reported in this Journal,[1] we have observed that the measured cross sections for photodissociation in the visible region were dependent upon the pressure of SO_2 used in the ion source. Since our previous work using the same ion source had shown no pressure effect on the photodissociation cross sections of N_2O^+,[2] this observation was unexpected. At source pressures in the 0.01 to 0.10 Torr range ($\sim 30\times$ the pressure used in gathering our previous SO_2^+ data) a significant effect on the photodissociation spectrum of Ar_2^+ had previously been observed in the same ion source, however.[3] This effect was interpreted in terms of collisional deactivation of vibrationally excited Ar_2^+, with a rate constant $\approx 12\%$ of Langevin. Thus, the pressure effect seen for SO_2^+ indicated some deactivation process occurring at a rate exceeding the theoretical upper limit for ion–molecular reactions. It therefore seemed important to make a systematic study of the processes involved and their precise rate constants.

II. EXPERIMENTAL METHOD

The ion photodissociation apparatus—a triple quadrupole system with coaxial irradiation of the ion beam by a flashlamp pumped dye laser—has been described in detail previously.[1] The first quadrupole transmitted only ions of a selected mass into the second quadrupole ("reactor quadrupole," with rf field only) where the only observable interaction with the laser beam occurred. The third quadrupole was adjusted to transmit either photoproduct ions or unreacted parent ions to the detector. Before beginning a systematic study of the pressure dependence of the photodissociation cross sections an MKS Baratron gauge equipped with a 1 Torr head was connected to one side of the ionization chamber via 1/4 in. o.d. (3/16 in. i.d.) tubing. Since sample gases flowed into the ionization chamber through a separate 1/4 in. o.d. tube connected at the opposite side of the chamber and the major escape path was through the 1/8 in. i.d. ion exit aperture (see the top half of Fig. 1), it was thought that the pressure measured in the Baratron head corresponded closely to that existing in the ionization region. There was no repeller in the ionization chamber.

Ions were produced by the impact of electrons accelerated through 50 V from a hot rhenium filament to the ionization chamber which they entered through a 1 mm hole. When the pressure in the ionization chamber was changed, the current through the filament was manually adjusted (in the opposite direction) to keep a constant ion beam current in the reactor quadrupole. Typically, the total emission from the filament was changed from 40 to $\leq 1.0\,\mu$A as the pressure in the ionization chamber was raised from 0.5 to 8.0 mTorr. This adjustment was intended to avoid changes in the ion beam profile and possible saturation effects on the ion-counting system which could have produced artificial pressure effects. No significant effect of changing *only* the filament emission on the photodissociation cross sections was observed.

In order to obtain quenching rate constants from the pressure dependence of the photodissociation cross sections it was necessary to determine the average residence time of the SO_2^+ ions in the ion source. For this purpose, about halfway through this study, a grid (82% transmitting Ni mesh) was installed between the filament and the ionization chamber, as shown in the top half of Fig. 1. This grid was normally biased slightly negative with respect to the filament until the arrival of a positive voltage pulse 0.4–0.5 μs wide from an EH 132 A-8 pulse generator, which caused a burst of electrons to enter the ionization chamber. A second pulse generator (Hewlett Packard 214 A), triggered by the first with a adjustable time delay, delivered a + 95 V pulse, 0.4–0.5 μs wide, to the ion accelerating plate located next to the ion exit hole in the ionization chamber. The timing sequence for the pulses is shown in the lower half of Fig. 1. This second pulse produced a dip in the peak of ion counts seen on the time-of-flight spectrum of the ions produced by the initial burst of electrons, as shown in Fig. 2. The time delay (measured on a Tektronix 511 oscilloscope) between the two voltage pulses which centered the dip in the top of the TOF peak was taken to equal the average residence time in the ionization chamber (Υ_i) plus the flight time of the ions between the ion exit hole and the accelerating plate (Υ_f):

$$\Upsilon_m = \Upsilon_i + \Upsilon_f. \quad (1)$$

 0021-9606/88/095553-08$02.10

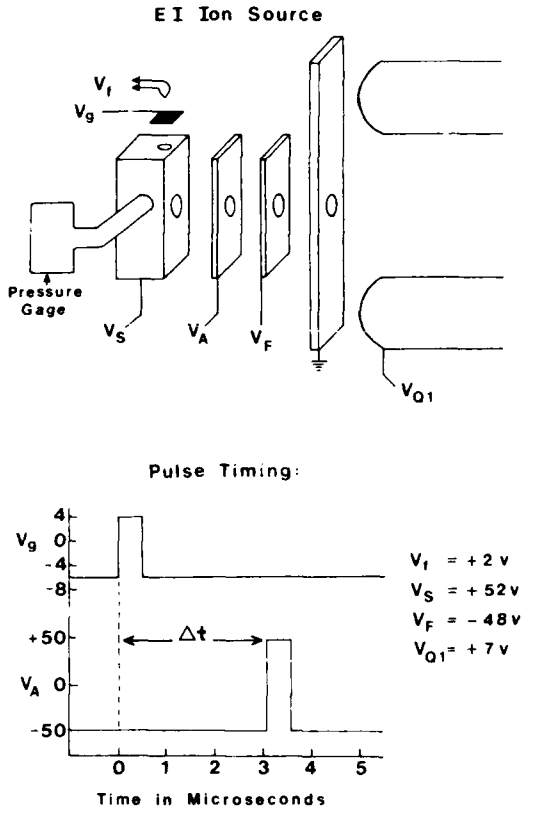

FIG. 1. Electron impact ion source (upper) and double-pulse timing sequence used to measure residence time in ion source (lower). V_f, V_g, V_S, V_A, and V_F designate the voltages applied to the filament, control grid, ionization chamber ("ion source"), ion accelerating plate, and focusing plate, respectively.

The flight time Υ_f was calculated from

$$\Upsilon_f = (2dm/eE)^{1/2}, \tag{2}$$

where d = the distance from the ion exit hole to the center of the accelerating plate $= 2.86\times10^{-3}$ m, E = the voltage gradient over that distance $= 3.50\times10^{4}$ V m^{-1}, and m = the mass of the SO_2^+ ions. The calculated value was $\Upsilon_f = 0.33$ μs.

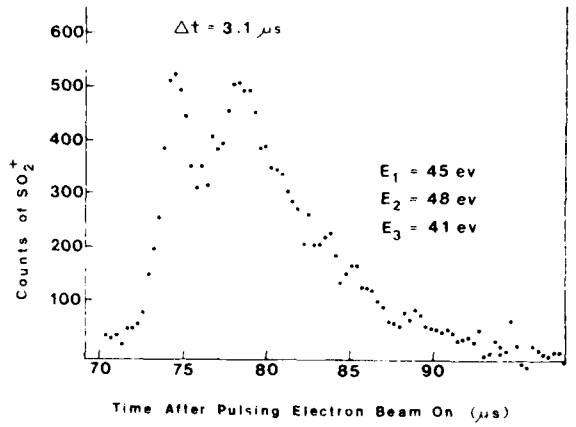

FIG. 2. Time-of-flight spectrum of SO_2^+ formed by pulsing electron beam on. Δt = time between pulsing electron beam on (V_g = +4 V) and applying +95 V pulse to ion accelerating plate (V_A). P = 0.7 mTorr (89% CO_2 + 11% SO_2). E_1, E_2, E_3 = ion kinetic energies in the source, reactor, and analyzer quadrupoles, respectively.

The values of Υ_m were found to increase linearly with the pressure in the ionization chamber. The best fit of the pressure dependence of the source residence times was given by

$$\Upsilon_s = 2.6(\pm0.2) + 0.17(\pm0.02)P, \tag{3}$$

where Υ_s is in μs and the pressure is in mTorr. The indicated error ranges are standard deviations from a least-squares fit to residence times determined at seven pressures ranging from 0.5$_9$ to 7.1 mTorr. Other equations tried, which were less accurate in fitting the observed pressure dependence, included: ln Υ_s vs P, Υ_s^{-1} vs P^{-1}, and Υ_s^{-1} vs $P^{1/2}$. The latter two functions, predicted to describe the mobility of ions for low, and for moderately strong, ratios of electric field to gas density (E/N), respectively,[4] predict a stronger pressure dependence than actually observed. For the sake of comparison, the residence time of neutral molecules in the ion source was 1.2 ms when $P = 3.2$ mTorr.

Photodissociation cross sections measured after modifying the ion source for the double-pulse measurements of residence times showed a significantly smaller dependence on pressure than those measured before the modifications. This difference may be due to the effect of the control grid (biased 33 V positive with respect to the filament in the quenching experiments performed after the measurement of the source residence times) on the electric field inside the source. The two sets of quenching data were made consistent by multiplying the values of Υ_s calculated from Eq. (3) by the factor 2.05 before plotting the data from the earlier experiments in Figs. 4 and 5.

Gas mixtures were prepared on a stainless steel vacuum line equipped with three 1 ℓ storage bulbs and four Bourdon tube pressure gages (0–1000 Torr range, smallest scale division = 10 Torr). In the case of $SO_2 + N_2O$ and $SO_2 + CO_2$ mixtures a measured amount of each gas was frozen from different storage bulbs into a single glass nipple, then flash vaporized into a third storage bulb which had previously been evacuated. In the case of $SO_2 + N_2$ known amounts of each gas were mixed by sudden expansion from their storage bulbs into the vacuum line, followed by a second rapid expansion into a third (evacuated) storage bulb. In this case the mixing was allowed to continue overnight. The compositions of the prepared mixtures, based on measured initial pressures, were: 80% N_2O + 20% SO_2; 89% CO_2 + 11% SO_2; and 89% N_2 + 11% SO_2. Mass spectral analyses run before and after using the mixtures confirmed these compositions within $<2\%$ except for the case of $N_2O + SO_2$, which appeared to change from 80% to 87% N_2O during the two day period in which that mixture was used. The gases used to make the mixtures were all of stated purities $\geq$99%; the SO_2, N_2O, and CO_2 were subjected to at least one freeze (in liquid N_2)–pump–thaw cycle to remove noncondensible impurities before use.

To confirm that the pressure in the ionization region was being measured accurately, and to obtain an estimate of the electric field present in the ionization region, a series of

Unclassified
SECURITY CLASSIFICATION OF THIS PAGE

REPORT DOCUMENTATION PAGE

1a. REPORT SECURITY CLASSIFICATION Unclassified	1b. RESTRICTIVE MARKINGS
2a. SECURITY CLASSIFICATION AUTHORITY	3. DISTRIBUTION / AVAILABILITY OF REPORT Approved for public release; Distribution Unlimited
2b. DECLASSIFICATION / DOWNGRADING SCHEDULE	
4. PERFORMING ORGANIZATION REPORT NUMBER(S) AFGL-TR-88-0143	5. MONITORING ORGANIZATION REPORT NUMBER(S)
6a. NAME OF PERFORMING ORGANIZATION Air Force Geophysics Laboratory 6b. OFFICE SYMBOL (If applicable) LID	7a. NAME OF MONITORING ORGANIZATION
6c. ADDRESS (City, State, and ZIP Code) Hanscom AFB Massachusetts 01731-5000	7b. ADDRESS (City, State, and ZIP Code)
8a. NAME OF FUNDING / SPONSORING ORGANIZATION 8b. OFFICE SYMBOL (If applicable)	9. PROCUREMENT INSTRUMENT IDENTIFICATION NUMBER
8c. ADDRESS (City, State, and ZIP Code)	10. SOURCE OF FUNDING NUMBERS PROGRAM ELEMENT NO. 61102F; PROJECT NO. 2303; TASK NO. G1; WORK UNIT ACCESSION NO. 12

11. TITLE (Include Security Classification)

Rate constants for quenching the $\tilde{A}\,^2A_2$ state of SO_2^+ by atmospheric gases

12. PERSONAL AUTHOR(S)
Timothy F. Thomas*, Fred Dale, John F. Paulson

13a. TYPE OF REPORT	13b. TIME COVERED	14. DATE OF REPORT (Year, Month, Day)	15. PAGE COUNT
Reprint	FROM _____ TO _____	1988 June 20	8

16. SUPPLEMENTARY NOTATION
*Department of Chemistry, University of Missouri-Kansas City Missouri 64110
-Reprinted from J. Chem Phys 88(9) 1 May 1988

17. COSATI CODES		
FIELD	GROUP	SUB-GROUP

18. SUBJECT TERMS (Continue on reverse if necessary and identify by block number)
Ion-Molecule Collisions, Collisional Quenching, Charge Transfer

19. ABSTRACT (Continue on reverse if necessary and identify by block number)

The effect of ion source pressure on the cross sections for photodissociation of SO_2^+ has been measured systematically at λ_{uv} = 4735 and 4795 Å. Using a Stern–Volmer treatment modified to account for the dependence of source residence time on pressure, rate constants have been measured for quenching the $\tilde{A}\,^2A_2$ ($v_1,v_2 = 3,3$) and $\tilde{A}\,^2A_2$($v_1,v_2 = 3,0$) states of SO_2^+ by N_2O, SO_2, CO_2, and N_2. With SO_2 and N_2O as quenchers the rate constants range between 1.0 and 6.5 times the theoretical thermal capture rate constants ("Langevin limit"). The occurrence of several resonant and many near-resonant charge transfer processes is proposed to explain the unusually large rate constants.

20. DISTRIBUTION / AVAILABILITY OF ABSTRACT ☐ UNCLASSIFIED/UNLIMITED ☒ SAME AS RPT. ☐ DTIC USERS	21. ABSTRACT SECURITY CLASSIFICATION Unclassified
22a. NAME OF RESPONSIBLE INDIVIDUAL John F. Paulson	22b. TELEPHONE (Include Area Code) (617) 377-3124 22c. OFFICE SYMBOL LID

DD FORM 1473, 84 MAR 83 APR edition may be used until exhausted. All other editions are obsolete.

SECURITY CLASSIFICATION OF THIS PAGE
Unclassified

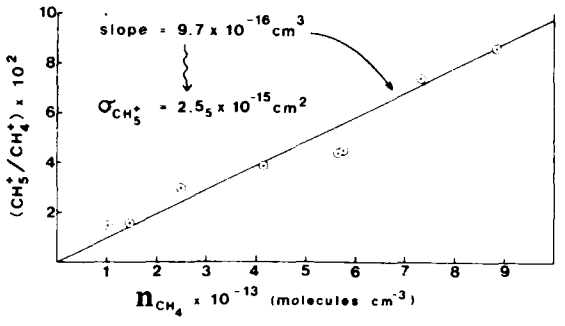

FIG. 3. Cross section measurement for $CH_4^+ + CH_4 \rightarrow CH_5^+ + CH_3$ in ion source of ion photodissociation spectrometer. $T \sim 50$ °C.

surements was made of the extent of the reaction

$$CH_4^+ + CH_4 \rightarrow CH_5^+ + CH_3 \qquad (4)$$

which occurred when pure (Research Grade) CH_4 was introduced into the ion source. These experiments were carried out immediately following the quenching experiments using the same operating conditions for the triple quadupole mass spectrometer with the following exceptions: the ion energy in the second quadrupole (E_2) was changed from 3.9 to 16 eV; the rf voltage on the second quadrupole was reduced from 400 to 210 VAC; and both reactant (CH_4^+) ion currents were measured on a Faraday cup located at the end of the third quadrupole using a Cary 31 electrometer.

The observed dependence of the ratio of product ion current to reactant ion current upon the concentration of CH_4 in the ion source is shown in Fig. 3. The cross section for reaction (4) was calculated from Eq. (5),

$$\left(\frac{CH_5^+}{CH_4^+}\right) = \sigma l\,[CH_4], \qquad (5)$$

where l = the distance from the electron beam in the center of the ionization region to the ion exit hole = 0.38 cm. The result was $\sigma = 25.5$ Å^2. Comparison of this value with the literature data on the dependence of the cross section on average kinetic energy of the reactant ions[5,6] leads to the following value for the electric field strength present in our ion source: $E = 8.1$ V/cm.

The preceding result was used to calculate a theoretical ion source residence time, using an equation by Field, Franklin, and Lampe[7] (although in our case the electric field was due to penetration of fields from the ion accelerating plate and filament grid instead of established by a repeller plate), yielding $\Upsilon_s = 2.5$ μs. This time agrees with our measured source residence time at the $P = 0$ limit, within our indicated experimental error.

III. RESULTS

Figures 4 and 5 show the effect of pressure in the ionization region upon the reciprocal of the measured photodissociation cross section for several gas mixtures and two irradiation wavelengths. The method of plotting the data is a modification of the classical Stern–Volmer treatment, taking into account the variation in source residence time reported in Sec. II. Equations for analyzing these data were

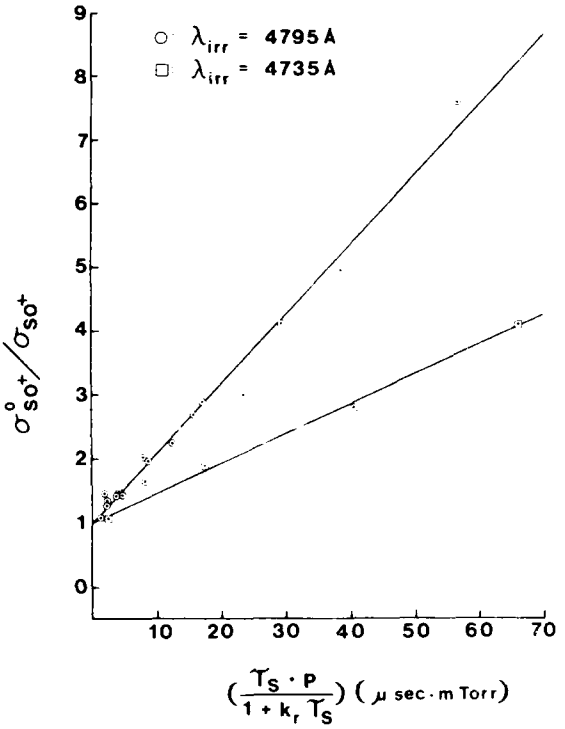

FIG. 4. Dependence of cross sections for $SO_2^+ + h\nu \rightarrow SO^+ + O$ on source pressure (P) and residence time (Υ_s). $\sigma^0_{SO^+}$ = limit of cross section when $p \rightarrow 0$; $k_r = 4.0 \times 10^4$ s^{-1}. For pure SO_2.

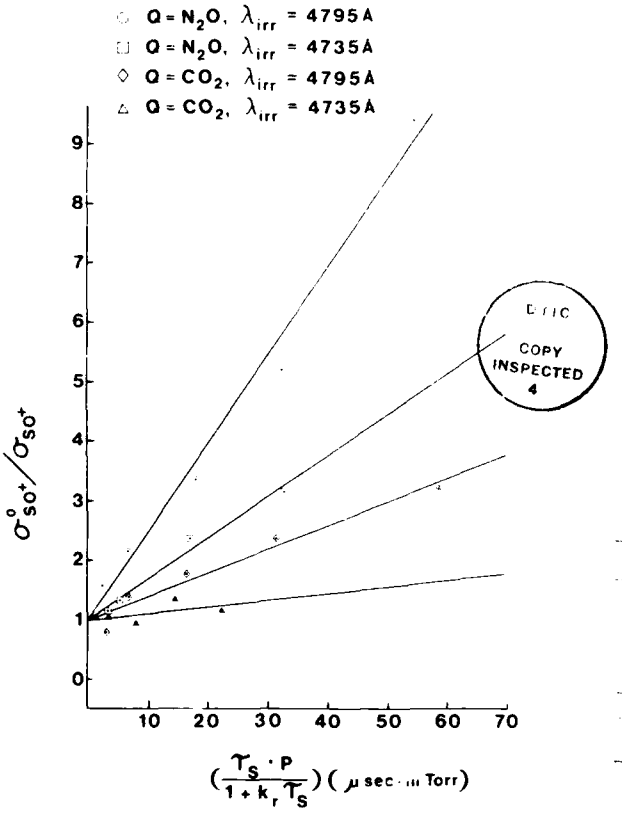

FIG. 5. Dependence of cross sections for $SO_2^+ + h\nu \rightarrow SO^+ + O$ on source pressure and residence time for mixed gases.

derived from the following scheme of fundamental processes occurring in the ion source:

Process	Rate	
$SO_2 + e^- \rightarrow SO_2^{+\dagger} + 2e$	$\alpha_1 i_{em}[SO_2]$,	(6)
$SO_2 + e^- \rightarrow SO_2^+ + 2e^-$	$\alpha_2 i_{em}[SO_2]$,	(7)
$Q + e \rightarrow Q^+ + 2e$	$\alpha_Q i_{em}[Q]$,	(8)
$SO_2^{+\dagger} + SO_2 \rightarrow SO_2^+ + SO_2^*$	$k_{SO_2}[SO_2^{+\dagger}][SO_2]$,	(9)
$SO_2^{+\dagger} + Q \rightarrow SO_2^+ + Q^*$	$k_r[SO_2^{+\dagger}][Q]$,	(10)
$SO_2^{+\dagger} + Q \rightarrow SO_2 + Q^+$	$k_{ce}[SO_2^{+\dagger}][Q]$,	(11)
$SO_2^{+\dagger} \rightarrow SO_2^+ + h\nu$	$k_r[SO_2^{+\dagger}]$,	(12)
$Q^+ + SO_2 \rightarrow SO_2^+ + Q$	$k_{rce}[Q^+][SO_2]$,	(13)
$SO^{+\dagger} \rightarrow (SO_2^{+\dagger})_{\text{ion beam}}$	$k_e[SO_2^{+\dagger}]$,	(14)
$SO_2^+ \rightarrow (SO_2^+)_{\text{ion beam}}$	$k_e[SO_2^+]$.	(15)

The first three processes shown are ionization by electron impact. The † designates an observable electronically excited state—in the case of the 4400–5200 Å portion of the photodissociation spectrum of SO_2^+ this refers to the metastable $\tilde{A}(^2A_2)$ state. The next three lines represent energy transfer processes, electronic (including charge transfer) and vibrational, which deplete the population of a particular energy level in $SO_2^{+\dagger}$ from which a transition originates for a given λ_{irr}. Q is the added gas whose quenching efficiency was measured. Step (12) allows for radiative decay from the metastable state. Steps (14) and (15) allow for escape from the ion source to the ion beam where the low density makes the rate of collisions insignificant.

Use of the steady state approximation for the concentration of the reactive intermediates in the above scheme yields the following expressions for the concentrations of $SO_2^{+\dagger}$ and SO_2^+ in the ion source:

$$[SO_2^{+\dagger}] = \frac{\alpha_1 i_{em}[SO_2]}{\beta + k_r + k_e} \tag{16}$$

and

$$[SO_2^+] = \frac{i_{em}}{k_e}\left\{\alpha_2[SO_2] + \alpha_Q[Q] + \frac{\beta\alpha_1[SO_2]}{\beta + k_r + k_e}\right\}, \tag{17}$$

where

$$\beta = k_{SO_2}[SO_2] + (k_r + k_{ce})[Q]. \tag{18}$$

For a given gas mixture, introduced into the ion source at different total pressures but fixed composition, one can make the following substitution in Eqs. (16)–(18): $[SO_2] = X_{SO_2} P/RT$ and $[Q] = X_Q P/RT$, in which X_{SO_2} and X_Q are the mole fractions of SO_2 and the quenching gas, respectively. Then,

$$\beta = \frac{P}{RT}[X_{SO_2} k_{SO_2} + X_Q(k_r + k_{ce})]. \tag{19}$$

The photodissociation cross sections previously reported for SO_2^+, as well as those measured in this work, were calculated using the total ion beam current in the laser–ion interaction region. For $\lambda_{irr} \geq 4187$ Å, however, only ions in the $\tilde{A}$ state (or higher) of SO_2^+ are capable of photodissociation. Thus, the observed cross sections are related to the true cross sections for processes originating in the $\tilde{A}$ state by

$$\sigma_{obs} = \left(\frac{[SO_2^{+\dagger}]\exp(-k_r t)}{[SO_2^{+\dagger}] + [SO_2^+]}\right)\cdot\sigma_{true}. \tag{20}$$

Equation (20) assumes the same relative population of the metastable ions in the ion beam as in the ion source except for a correction factor for radiative decay.[8] Substituting Eqs. (16)–(18) into Eq. (20) gives

$$\sigma_{obs} = \frac{k_e\alpha_1\sigma_{true}\exp(-k_r t)}{(k_r + k_e + \beta)\{\alpha_1 + \alpha_2 + (\alpha_Q[Q]/[SO_2])\}}. \tag{21}$$

In the limit of zero pressure (for fixed composition) $\beta \rightarrow 0$, and

$$\sigma^0_{obs} = \frac{k_e\alpha_1\sigma_{true}\exp(-k_r t)}{(k_r + k_e)\{\alpha_1 + \alpha_2 + (\alpha_Q[Q]/[SO_2])\}}. \tag{22}$$

Dividing Eq. (22) by Eq. (21) yields

$$\frac{\sigma^0_{obs}}{\sigma_{obs}} = 1 + \frac{\beta}{k_r + k_e}. \tag{23}$$

Using Eq. (19) and $k_e = \Upsilon_s^{-1}$, where Υ_s is given by Eq. (3), converts Eq. (23) into the equation used to fit the pressure dependence of the photodissociation cross sections:

$$\frac{\sigma^0_{obs}}{\sigma_{obs}} = 1 + \frac{[X_{SO_2} k_{SO_2} + X_Q(k_r + k_{ce})]}{RT} \times\left(\frac{\Upsilon_s}{1 + k_r\Upsilon_s}\right)P. \tag{24}$$

The experimental data obtained in the study are plotted in Figs. 4 ($X_Q = 0$) and 5 ($X_Q \neq 0$), using the previously determined value of $k_r = 4.0 \times 10^4$ s^{-1}. The variables plotted are the same as in the classical Stern–Volmer treatment of fluorescence quenching, except that the pressure in the ion source is modified by a factor which accounts for the nonconstant residence time: $\Upsilon_s/(1 + k_r\Upsilon_s)$. Without this factor σ^0/σ vs P plots showed considerable curvature for pure SO_2 and for the $SO_2 + N_2O$ mixture. Ten points obtained using the $SO_2 + N_2$ mixture (five at each wavelength) were omitted from Fig. 5 for the sake of clarity. Values of k_{SO_2} were obtained from the slopes of the least-squares lines shown in Fig. 4, using $T = 323$ K in Eq. (24). These values of k_{SO_2} were then combined with the slopes of the lines shown in Fig. 5, and with the unplotted data for $SO_2 + N_2$, to obtain values for $k_r + k_{ce}$ for $Q = N_2O$, CO_2, and N_2. The resulting rate constants, in molecular units, are shown in Table I. The indicated uncertainties are obtained from the standard deviations of the slopes of the lines in Figs. 4 and 5.

The rate constants were converted into the quenching cross sections, shown in the last column of Table I, using the relation

$$\sigma_Q = k/\bar{v}. \tag{25}$$

Here $\bar{v}$, the average velocity toward the exit hole of the ions in the ionization region, was estimated from l/Υ_s^0, where l was defined in Sec. II and Υ_s^0 is the source residence time at the limit of zero pressure. The resulting value for SO_2^+ is $\bar{v} = 1.4_6 \times 10^5$ cm/s.

A short series of measurements of the pressure depen-

TABLE I. Quenching rate constants for SO_2^+ ($\tilde{A}\,^2A_2$).

Quencher	$10^{9}\times k_{SO_2}$ ($cm^3\,s^{-1}$)	$10^{9}\times(k_v+k_{ex})$ ($cm^3\,s^{-1}$)	σ_Q(Å^2)
$\lambda_{irr}=4735$ Å			
SO_2	1.55 ± 0.06		106 ± 4
N_2O		$2.52\pm.0.29$	173 ± 20
CO_2		$0.22+0.32$	15 ± 22
N_2		-0.36 ± 0.20	-25 ± 14
$\lambda_{irr}=4795$ Å			
SO_2	3.63 ± 0.12		249 ± 38
N_2O		5.38 ± 0.45	368 ± 31
CO_2		1.08 ± 0.20	74 ± 14
N_2		0.47 ± 0.20	32 ± 14

dence of the photodissociation cross sections was made in the UV spectrum of SO_2^+, using pure SO_2 and $\lambda_{irr}=3192$ Å. The cross sections were found to *increase* with increasing source pressure (in contrast to the data in the visible region) up to $P\sim3$ mTorr, where a maximum was reached. Above 3 mTorr the cross sections began to decrease slowly with pressure; at higher pressures the value of $d(\sigma'')/\sigma)/d(P\cdot\Upsilon_s)$ approximated that found for the 89% N_2 + 11% SO_2 mixtures at $\lambda_{irr}=4795$ Å. Since the major transition occurring at 3192 Å is thought to be $\tilde{X}\,^2A_1\rightarrow\tilde{C}\,^2B_1$, the low pressure results seem to confirm step (9), which augments the population of the $\tilde{X}$ state of SO_2^+, in the proposed quenching mechanism. The weaker pressure effect above 3 mTorr is consistent with a contribution at 3192 Å from an $\tilde{X}\rightarrow\tilde{C}$ transition originating from an excited vibrational level (we estimate that the $1_1^4 2_4^4$, $1_0^3 2_4^2$, and $1_0^2 2_4^4$ bands, e.g., would lie near 3192 Å). Another possible contributor would be a second electronic transition, such as $\tilde{A}\,^2I_2\rightarrow\tilde{D}\,^2B_2$ (for which we predict an origin of $\lambda_{0,0}\simeq3792$ Å).

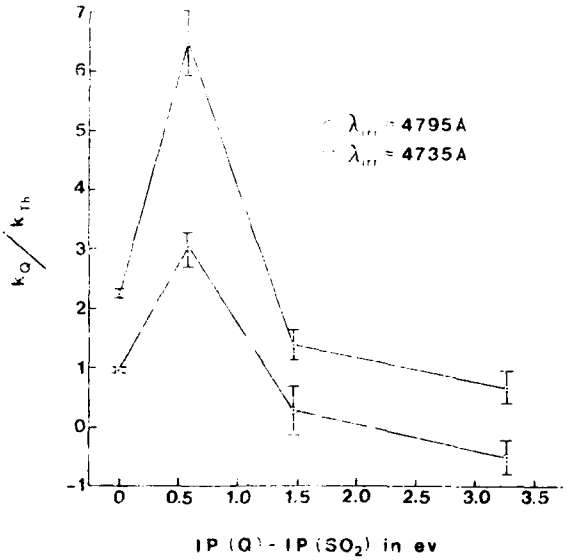

FIG. 6. Quenching rate constants as a function of difference in first ionization potentials of quencher and SO_2. "k_Q" = k_{ex} for pure SO_2; $k_Q=k_v+k_{ex}$ for Q = N_2O, CO_2, and N_2.

TABLE II. Selected ionization potentials and vibrational frequencies.[a]

Specie	Electronic state	IP(eV)	$\tilde{\nu}_1$(cm^{-1})	$\tilde{\nu}_2$(cm^{-1})	$\tilde{\nu}_3$(cm^{-1})
SO_2	$\tilde{X}\,^1A_1$	0	1167[j]	526[j]	1381[j]
SO_2^+	$\tilde{X}\,^2A_1$	12.311[b]	(1151)[c]	454[c]	(1362)[c]
SO_2^+	$\tilde{A}\,^2A_2$	13.030[d]	953[c]	499[c]	(1127)[c]
N_2O	$\tilde{X}\,^1\Sigma^+$	0	1285	589	2224
N_2O^+	$\tilde{X}\,^2\Pi_{3/2}$	12.886[e]	1126.5[f]	456.8[f]	1737.6[f]
N_2O^+	$\tilde{X}\,^2\Pi_{1/2}$	12.902[e,f]	1126.5[f]	456.8[f]	1737.6[f]
CO_2	$\tilde{X}\,^1\Sigma_g^+$	0	1333	667	2349
CO_2^+	$\tilde{X}\,^2\Pi_{3/2}$	13.776[g]	1266[g]	508[g]	1472[g]
N_2	$\tilde{X}\,^1\Sigma_g^+$	0	2359[h]		
N_2^+	$\tilde{X}\,^2\Sigma_g^+$	15.580[i]	2207[h]		

[a] All vibrational frequencies are from Ref. 26 unless otherwise noted; corrections for anharmonicity were applied in the case of SO_2 and SO_2^+ ($\tilde{A}$) only.
[b] Calculated from the fourth IP = 15.992 ± 0.003 eV for SO_2 (Ref. 27) and the tentatively assigned $\lambda_{0,0}=3368\pm1$ Å for $\tilde{A}\,^2A_2\rightarrow\tilde{C}\,^2B_1$ in SO_2^+ (Ref. 1). Previously reported values for the first IP of SO_2 are 12.30$_6$ ± 0.01 (Ref. 12) and 12.348 ± .002 eV (Ref. 28).
[c] From Ref. 1. ν_1 and ν_3 in the $\tilde{X}$ state were taken to be the same as for SO_2 (Ref. 26) and ν_3 in the $\tilde{A}$ state was estimated assuming $\tilde{\nu}_3'/\tilde{\nu}_3''=1.183$.
[d] Calculated from the fourth IP = 15.992 ± 0.003 eV for SO_2 (Ref. 27) and $\lambda_{0,0}=4187\pm1$ Å for $\tilde{A}\,^2A_2\rightarrow\tilde{C}\,^2B_1$ in SO_2^+ (Ref. 1).
[e] ± 0.002 eV, from Ref. 29. Other reported values are 12.889 (Ref. 30) and 12.893 ± .005 eV (Ref. 31).
[f] The $\tilde{\nu}_2$ and the $^2\Pi_{3/2}$–$^2\Pi_{1/2}$ splitting are from Ref. 25.
[g] From Ref. 32.
[h] From Ref. 33.
[i] From Ref. 34.
[j] From Ref. 35.

IV. DISCUSSION

The ratios of the experimentally determined quenching rate constants to theoretical rate constants are plotted vs the differences between the first ionization potentials of the quenchers and SO_2 in Fig. 6. The "theoretical" rate constants are thermal capture rate constants for collisions of SO_2^+ and the quencher, calculated using the parametrization of Su and Chesnavich,[10] which was estimated by those authors to be accurate to $<3\%$. We used the following polarizabilities and dipole moments in the calculations: $\alpha=4.28(SO_2)$, $3.03(N_2O)$, $2.91(CO_2)$, and $1.74(N_2)$ Å^3; $\mu=1.63(SO_2)$ and $0.16(N_2O)$ D.[11] The strong dependence of k_Q/k_{Th} on the ionization potential of the quencher indicates that electronic energy transfer is the major pathway for quenching, at least for Q = SO_2 and N_2O. The "peak" observed in Fig. 6 matches well with the location of the $\tilde{A}$ state of SO_2^+, which lies 0.719$_5$ eV above the $\tilde{X}$ state (see Table II). This observation provides further confirmation that it is the $\tilde{A}$ state of SO_2^+ which is being quenched at $\lambda_{irr}=4735$ and 4795 Å.

A brief review of recent literature on the quenching of excited states of ions by small neutral molecules shows the following trends:

(a) Quenching rate constants usually increase with increasing vibrational quantum number in the donor.[13–17]

(b) Ions in electronically excited states react more rapidly than the corresponding ions in ground electronic states.[18–20]

(c) An applied electric field (increasing ion velocity), has

only a small effect on the rate of some exothermic charge transfer reactions of O_2^+ [17,19,21] but a stronger effect on charge transfer from CO_2^+, N_2O^+, and SO_2^+.[22] It is generally assumed, however, that the rate constant never exceeds k_{Th}.

It has also commonly been accepted that a small ΔE and large Franck–Condon factors are necessary for the quenching process to be fast.[14,15,37,38] In the present study the ions being quenched are highly vibrationally excited ($v_1 = 3$ for both wavelengths used, plus $v_2 = 3$ when $\lambda_{irr} = 4795$ Å) as well as electronically excited so that large quenching rate constants would be expected if ΔE is small and the Franck–Condon factors are favorable. Figure 6 also shows that all k_Q's increase when v_2 is increased from 0 ($\lambda_{irr} = 4735$ Å) to 3 ($\lambda_{irr} = 4795$ Å).

In the case where $Q = N_2O$ the following processes are calculated, using the data shown in Table II, to provide essentially resonant pathways for quenching by charge exchange[23]:

$$SO_2^+(\tilde{A}\,^2A_2,330) + N_2O \rightarrow SO_2(340) + N_2O^+(\tilde{X}\,^2\Pi_{3/2},000), \quad \Delta E = 108 \text{ cm}^{-1}, \tag{26}$$

$$SO_2^+(\tilde{A}\,^2A_2,300) + N_2O \rightarrow SO_2(310) + N_2O^+(\tilde{X}\,^2\Pi_{3/2},000), \quad \Delta E = -6 \text{ cm}^{-1}. \tag{27}$$

Not only is ΔE nearly zero, within the combined uncertainty (± 50 cm^{-1}) of the two ionization potentials used to calculate the quantity, but the Franck–Condon factors should be large also because $\Delta v_1 = 0$ and $\Delta v_2 = 1$ to 8 for the strongest peaks in the first band of the photoelectron spectrum of SO_2[12] and the largest Franck–Condon factor for ionization of N_2O corresponds to the $X\,^1A_1 \rightarrow \tilde{X}\,^2\Pi_{3/2},000$ transition.[24]

In addition to reactions (26) and (27), 43 exothermic charge transfer processes are predicted to be possible from the $v_1v_2v_3 = 330$ vibrational level and 34 processes from the 300 level of the $\tilde{A}$ state of SO_2^+, to yield either the $\tilde{X}\,^2\Pi_{3/2}$ or $\tilde{X}\,^2\Pi_{1/2}$ states of N_2O^+, subject to the restriction that $v_1 \leqslant 3$ and $v_2 \leqslant 5$ in the neutral SO_2 product. Still more exothermic processes may be written yielding N_2O^+ with $v_2 = 1$ or 2, which vibrational levels are split by the Renner effect into ten states lying within 0.139 eV (1122 cm^{-1}) of $\tilde{X}\,^2\Pi_{3/2},000$.[25] One example of such a process is

$$SO_2^+(\tilde{A}\,^2A_2,330) + N_2O \rightarrow SO_2(330) + N_2O^+(\tilde{X}^{ev}\Sigma^{(+)}_{1/2},010), \quad \Delta E = +27 \text{ cm}^{-1}, \tag{28}$$

where the notation used for the spin-vibronic level of N_2O^+ is taken from Callomon and Creutzberg.[25] The rate constants listed under the heading "$k_v + k_{ce}$" for $Q = N_2O$ in Table I are the sums of the rate constants for all processes which depopulate the previously indicated excited states. Based on the results obtained with $Q = CO_2$ and N_2 (see below), however, we conclude that $k_{ce} \gg k_v$ when $Q = N_2O$ or SO_2.

In the case where $Q = SO_2$, step (9) in the reaction scheme proposed above includes two distinct processes. The first process is collision-induced internal conversion of SO_2^+ from the $\tilde{A}\,^2A_2$ state to the $\tilde{X}\,^2A_1$ state with the decrease in electronic energy of the ion equaling the increase in its vibrational energy. Examples of this process for the two vibronic states of SO_2^+ whose quenching rates were measured in our study are

$$SO_2^+(\tilde{A}\,^2A_2,330) + SO_2 \rightarrow SO_2^+(\tilde{X}\,^2A_1,590) + SO_2, \quad \Delta E = -111 \text{ cm}^{-1}, \tag{29}$$

$$SO_2^+(\tilde{A}\,^2A_2,300) + SO_2 \rightarrow SO_2^+(\tilde{X}\,^2A_1,560) + SO_2, \quad \Delta E = -90 \text{ cm}^{-1}. \tag{30}$$

Since $\Delta v_1 = +2$ for the ion, the Franck–Condon factors may not be as large as for reactions (26) and (27). Also, the calculated ΔE's may not be very accurate since no anharmonicity constants were available to use for predicting vibrational energies in the $\tilde{X}$ state of SO_2^+.

The second quenching process when $Q = SO_2$ is charge transfer. Example reactions which are nearest to resonance (subject to the restrictions $\Delta v_1 = \Delta v_2 = 0$ in the donor and $v_1 \leqslant 5$, $v_2 \leqslant 10$ in the product ion) are

$$SO_2^+(\tilde{A}\,^2A_2,330) + SO_2 \rightarrow SO_2(330) + SO_2^+(\tilde{X}\,^2A_1,260), \quad \Delta E = +21 \text{ cm}^{-1}, \tag{31}$$

$$SO_2^+(\tilde{A}\,^2A_2,300) + SO_2 \rightarrow SO_2(300) + SO_2^+(\tilde{X}\,^2A_1,410), \quad \Delta E = -80 \text{ cm}^{-1}. \tag{32}$$

Subject to the same restrictions, another exothermic 31 and 32 state-to-state reactions may be written for $v_1v_2v_3 = 330$ and 300 levels of SO_2^+ ($\tilde{A}$), respectively.

In the case where $Q = CO_2$ charge transfer from the $\tilde{A}$ state of SO_2^+ is endothermic by 6013 ± 50 cm^{-1}. Thus, $k_{ce} \ll k_v$ would be expected. This expectation is supported by the fact that k_Q (4795 Å) $\sim 5 \cdot k_Q$ (4735 Å) reflecting the greater ease of transferring a quantum from the low energy bending mode ($\tilde{\nu}_2$) via

$$SO_2^+(\tilde{A}\,^2A_2,330) + CO_2 \rightarrow SO_2^+(\tilde{A}\,^2A_2,320) + CO_2(010), \quad \Delta E = +251 \text{ cm}^{-1} \tag{33}$$

than from the higher energy symmetric stretching mode via

$$SO_2^+(\tilde{A}\,^2A_2,300) + CO_2 \rightarrow SO_2^+(\tilde{A}\,^2A_2,200) + CO_2(100), \quad \Delta E = +421 \text{ cm}^{-1}. \tag{34}$$

It is also possible that quenching by CO_2 could occur via collision-induced internal conversion, analogous to reactions (29) and (30). It is not clear, however, why the rate constant for internal conversion should decrease by factors of 3.4 (at 4795 Å) and 7 (at 4735 Å) when the quencher is changed from SO_2 to CO_2. *A simpler interpretation of all our data is that the faster quenching by SO_2 and N_2O proceeds predominantly by charge transfer and that the results obtained for CO_2 measure the combined rate of V–V energy transfer and collision-induced internal conversion.*

The still smaller quenching rate constants obtained for $Q = N_2$ reflect the fact that the transfer of a single vibrational quantum would be endothermic by an amount much greater than $3/2\,RT$ (340 cm^{-1}):

$$SO_2^+(\tilde{A}\,^2A_2,330) + N_2 \rightarrow SO_2^+(\tilde{A}\,^2A_2,230) + N_2(1), \quad \Delta E = +1465 \text{ cm}^{-1}. \tag{35}$$

The negative value of the rate constant for quenching the $v_1v_2v_3 = 300$ level of the $\tilde{A}$ state of SO_2^+ is probably real, resulting from the rate of populating it by collision from

TABLE III. Selected charge transfer rate constants exceeding Langevin.

No.	Reaction	T(K)	$KE_{c.m.}$ (eV)	k_{cc}/k_{Th}	Method	Reference
(1)	$Ar_2^+ + CS_2 \rightarrow 2Ar + CS_2^+$	300	0.55	1.26 ± 0.06	SIFT-DRIFT	36
(2)	$D_2^+ (v=1) + N_2 \rightarrow D_2 + N_2^+$	~400	1.0	1.48 ± 0.37	PIRFG[b]	37
(3)	$H_2^+ (v=1) + N_2 \rightarrow H_2 + N_2^+$	~400	1.0	1.60 ± 0.40	PIRFG[b]	37
(4)	$N_2^+ (\tilde{B}\,^2\Sigma_u^+, v=1) + N_2 \rightarrow N_2 + N_2^+$	300	···	1.83 ± 0.28	FDQ[c]	16
(5)	$NO^+ (\tilde{a}\,^3\Sigma^+, v=2) + Ar \rightarrow NO + Ar^+$	~300	1.4	2.06	TESICO[d]	38
(6)	$H_2^+ (v=0) + CO \rightarrow H_2 + CO^+$	~400	1.0	2.17 ± 0.54	PIRFG	37
(7)	$SO_2^+ (\tilde{A}\,^2A_2, v_1v_2 = 33) + SO_2 \rightarrow SO_2 + SO_2^+$	323	0.7_7[e]	$2.2_5 \pm 0.07$	IPDS[e]	This work
(8)	$SO_2^+ (\tilde{A}\,^2A_2, v_1v_2 = 30) + N_2O \rightarrow SO_2 + N_2O^+$	323	0.6_3[e]	$3.0_4 \pm 0.35$	IPDS	This work
(9)	$D_2^+ (v=0) + CO \rightarrow D_2 + CO^+$	~400	1.0	$3.2_2 \pm 0.80$	PIRFG	37
(10)	$SO_2^+ (\tilde{A}\,^2A_2, v_1v_2 = 33) + N_2O \rightarrow SO_2 + N_2O^+$	323	0.6_3[e]	$6.4_4 \pm 0.54$	IPDS	This work

[a] Selected ion flow tube with electric drift field added. Ions produced by electron impact.
[b] Ions produced by photoionization in radio frequency ion guide, then beamed through a scattering cell filled with neutral reactant.
[c] From measurement of fluorescence decay rate as function of pressure of quenching gas.
[d] Threshold electron–secondary ion coincidence technique, with mass analysis of products from reaction of ion beam with neutral gas. k_{cc} is derived from a cross section calculated using the theoretical method of Rapp and Francis (Ref. 39).
[e] Ion photodissociation spectroscopy. The $KE_{c.m.}$ shown is an average value; the full range of values for ions formed in our ion source is $KE_{c.m.} = 0 \rightarrow 1.54$ eV when Q = SO_2 and $0 \rightarrow 1.26$ eV when Q = N_2O.

levels with $v_2 > 0$ being faster than the rate of depopulating it by removing a quantum from $v_1 = 3$. This effect of collision on the cascading from higher to lower energy levels does, of course, complicate the interpretation of all our data, but we believe it to be of minor importance in the cases of the larger rate constants measured.

As mentioned above it is often assumed that the thermal capture rate constants calculated by equations such as Su and Chesnavich's[10] provide an upper limit to experimentally determined rate constants for ion–molecule reactions. The results which we show in Table I and Fig. 6, however, exceed that upper limit by up to a factor of 6.5. It must be acknowledged that our k_Q's are not strictly thermal rate constants, since our SO_2^+ ions acquire a kinetic energy of $\leqslant 3.08$ eV while being accelerated out of our ion source by the field penetrating from the ion accelerating plate. We feel, however, that the effect of ion kinetic energy is unlikely to be large enough to entirely account for the large k_Q/k_{Th} ratios we observed. Of greater significance is the combined effect of vibrational and electronic excitation and the existence of many resonant or near-resonant channels by which charge transfer can occur.

To put our results in perspective three of our rate constants are compared in Table III with seven other recently determined rate constants which exceed k_{Th} by at least 25%. In all cases except the first one specific vibronic states were monitored. Most measurements of the rate of ion–molecule reactions yield rate constants averaged over many vibrational states, and possibly even over several electronic states, thus obscuring any very fast resonant processes. The very strong enhancement of rate constants for processes having $\Delta E < RT$ ($\sim 210\ cm^{-1}$ in our case) has been shown by Kato *et al.* who calculate that 50% of reaction (5) in Table III proceeds via the state specific process:

$$NO^+ (\tilde{a}\,^3\Sigma^+, v=2) + Ar \rightarrow NO(\tilde{X}\,^2\Pi_{1/2}, v=1) + Ar^+ (^2P_{3/2}), \quad \Delta E = +137\ cm^{-1} \qquad (36)$$

although a total of 28 channels were energetically attainable at the collision energy used. The model used in the calculation of Kato *et al.* applies to charge transfer occuring via a simple electron jump mechanism at large interaction distances. This model would appear to be appropriate to describe the major part of the quenching of $SO_2^+ (\tilde{A}\,^2A_2)$ by N_2O and by SO_2 and, as shown above, a number of channels exist in these cases which have even smaller ΔE's than does Eq. (36).

Based on our results and the above considerations, we suggest that many more reactions having $k_{cc} \gg k_{Th}$ can be discovered using recently developed techniques for studying state-to-state reactions between ions and molecules in which $\Delta E < RT$.

ACKNOWLEDGMENTS

The experimental work reported here was carried out at the Air Force Geophysics Laboratory while T.F.T. was an AFOSR-URRP Visiting Professor there. Support by Air Force Systems Command Contract No. F19628-84-K-0038 during the subsequent period of data analysis and manuscript preparation is gratefully acknowledged.

[1] T. F. Thomas, F. Dale, and J. F. Paulson, J. Chem. Phys. **84**, 1215 (1986).
[2] T. F. Thomas, F. Dale, and J. F. Paulson, J. Chem. Phys. **67**, 793 (1977).
[3] T. L. Rose, D. H. Katayama, J. A. Welsh, and J. F. Paulson, J. Chem. Phys. **70**, 4542 (1979).
[4] E. W. McDaniel and E. A. Mason, *The Mobility and Diffusion of Ions in Gases* (Wiley, New York, 1973), pp. 121–2.
[5] L. Friedman, in *Ion–Molecule Reactions in the Gas Phase*, Advances in Chem. Ser. No. 58 (American Chemical Society, Washington, D.C., 1966), p. 101.
[6] A. Giardini-Guidoni and L. Friedman, J. Chem. Phys. **45**, 937 (1966).
[7] F. H. Field, J. L. Franklin, and F. W. Lampe, J. Am. Chem. Soc. **79**, 2419 (1957).
[8] Under typical operating conditions t, the average flight time from the source to the region where photodissociation occurred (the center of the reactor quadrupole) was $\sim 48\ \mu s$. Using the previously determined value of $k_r = 4.0 \times 10^4\ s^{-1}$ (Ref. 9) gives $\exp(-k_r t) = 0.15$; thus, the previously published cross sections should be multiplied by 6.8 in the visible region to compensate for radiative decay from the metastable state formed in the ion source.

[9]T. F. Thomas, F. Dale, and J. F. Paulson, J. Chem. Phys. **79**, 4078 (1983).
[10]T. Su and W. J. Chesnavich, J. Chem. Phys. **76**, 5183 (1982).
[11]C. G. Gray and K. E. Gubbins, *Theory of Molecular Fluids. Vol. I. Fundamentals* (Oxford University, Oxford, 1984), Appendix D.
[12]J. H. D. Eland and C. J. Danby, J. Mass Spectrom. Ion Phys. **1**, 111 (1968).
[13]V. E. Bondybey and T. A. Miller, J. Chem. Phys. **69**, 3597 (1978).
[14]D. H. Katayama, T. A. Miller, and V. E. Bondybey, J. Chem. Phys. **72**, 5469 (1980).
[15]D. H. Katayama and J. A. Welsh, J. Chem. Phys. **79**, 3627 (1983); Chem Phys. Lett. **106**, 74 (1984).
[16]J. Jolly and A. Plain, Chem. Phys. Lett. **100**, 425 (1983).
[17]H. Bohringer, M. Durup-Ferguson, D. W. Fahey, F. C. Fehsenfeld, and E. E. Ferguson, J. Chem. Phys. **79**, 4201 (1983).
[18]J. Glosik, A. B. Rakshit, N. D. Twiddy, N. G. Adams, and D. Smith, J. Phys. B **11**, 3365 (1978).
[19]W. Lindinger, D. L. Albritton, M. McFarland, F. C. Fehsenfeld, and A. L. Schmeltekopf, J. Chem. Phys. **62**, 4101 (1975).
[20]T. Ibuki and N. Sugita, J. Chem. Phys. **79**, 5392 (1983); **80**, 4625 (1984).
[21]I. Dotan, Chem. Phys. Lett. **75**, 509 (1980).
[22]M. Durup-Ferguson, H. Bohringer, D. W. Fahey, and E. E. Ferguson, J. Chem. Phys. **79**, 265 (1983).
[23]The "330" in reaction (26) means $v_1 = 3$, $v_2 = 3$, $v_3 = 0$ quanta in the three vibrational modes of SO_2^+, and so forth through subsequent reactions.
[24]H. M. Rosenstock, Int. J. Mass Spectrom. Ion Phys. **7**, 33 (1971).
[25]J. H. Callomon and F. Creutzberg, Phil. Trans. R. Soc. London Ser. A **277**, 157 (1974).
[26]T. Shimanouchi, *Table of Vibrational Frequencies*, Natl. Stand. Ref. Data Ser., Natl. Bur. Stand. No. 39 (U.S. GPO, Washington, D.C., 1972), Vol. 1.
[27]D. R. Lloyd and P. J. Roberts, Mol. Phys. **26**, 225 (1973).
[28]J. Ericson and C. Y. Ng, J. Chem. Phys. **75**, 1650 (1981).
[29]J. Berkowitz and J. H. D. Eland, J. Chem. Phys. **67**, 2740 (1977).
[30]Y. Tanaka, A. S. Jursa, and F. J. LeBlanc, J. Chem. Phys. **32**, 1205 (1960).
[31]C. R. Brundle and D. W. Turner, Int. J. Mass Spectrom. Ion Phys. **2**, 195 (1969).
[32]A. W. Potts and G. H. Fattahallah, J. Phys. B **13**, 2454 (1980).
[33]K. P. Huber and G. Herzberg, *Molecular Spectra and Structure. IV. Constants of Diatomic Molecules* (Van Nostrand Reinhold, New York, 1979).
[34]M. Ogawa and Y. Tanaka, Can. J. Phys. **40**, 1593 (1962).
[35]R. D. Shelton, A. H. Nielson, and W. H. Fletcher, J. Chem. Phys. **21**, 2178 (1953).
[36]R. J. Shul, R. Passarella, X. L. Yang, R. G. Keesee, and A. W. Castleman, Jr., J. Chem. Phys. **87**, 1630 (1987).
[37]S. L. Anderson, T. Turner, B. H. Mahan, and Y. T. Lee, J. Chem. Phys. **77**, 1842 (1982).
[38]T. Kato, K. Tanaka, and I. Koyano, J. Chem. Phys. **79**, 5969 (1983).
[39]D. Rapp and W. E. Francis, J. Chem. Phys. **37**, 2631 (1962).